Experimental testing of composite T-Joints

Jean-Baptiste R. G. Souppez

Published online: 20 Aug 2024.

Submit your article to this journal ⬚

View related articles ⬚

View Crossmark data ⬚

Experimental testing of composite T-Joints

Jean-Baptiste R. G. Souppez

Mechanical, Biomedical and Design Engineering Department, School of Engineering and Technology, College of Engineering and Physical Sciences, Aston University, Birmingham, UK

ABSTRACT

Composite T-joints are adhesively bonded joints between a base plate and a panel normal to it. These are crucial, yet, they remain a structural weakness of marine composite structures. A new T-joint configuration, namely, bonding ties, has recently emerged but has never been experimentally characterised. Moreover, honeycomb cores have been favoured over foam for high-performance applications, but the former remains comparatively understudied. Consequently, this paper undertakes the mechanical testing of both foam and honeycomb-cored T-joints, using four configurations: resin fillets, bonding angles, bonding angles with fillets and bonding ties. The results show that (i) peel strength is independent of the core employed; (ii) both resin fillets and bonding ties achieve the lowest peel strength, and thus, bonding ties are not recommended; (iii) for foam-cored T-joints bonding angles and bonding angles with fillets respectively yield a 42% and 96% increase in peel strength compared to resin fillets; and (iv) for honeycomb-cored T-joints, an increase in peel strength of 46% and 84% compared to resin fillets is achieved for bonding angles and bonding angles with fillets, respectively. These findings provide novel insights into the strength of composite T-joints and may inform regulatory developments, future numerical studies and the design of marine T-joints.
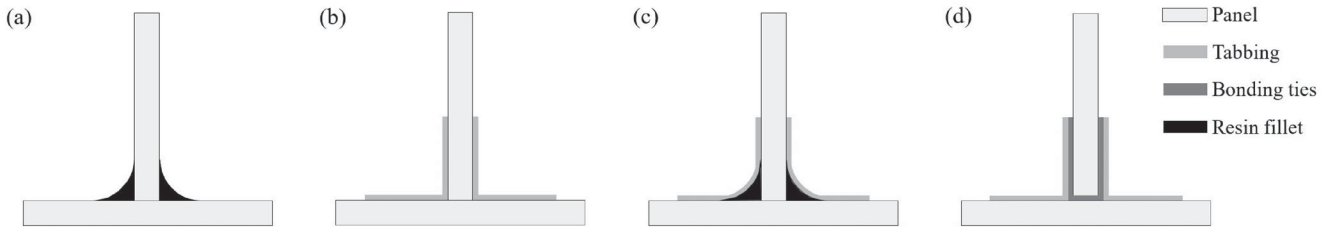
1. Introduction

Composite T-joints (or tee joints) are adhesively bonded structural joints comprising a base plating (e.g. single skin or cored hull shell or deck) and a panel normal to it (e.g. cored bulkhead). Such joints are crucial in marine applications, for instance, in joining the bulkheads to the hull plating and deck. This allows for load transfer and contributes to the structural stiffness of the structure, as well as its survivability in the case of watertight bulkheads (Dharmawan et al. 2004; Li et al. 2006; Delzendehrooy et al. 2022; Truelock et al. 2022). However, despite the structural significance of adhesively bonded T-joints in composite structures, these remain a structural weakness where failure is likely to originate (Bai et al. 2019). Indeed, the interface between the base plating and bulkhead has been consistently identified as being the origin of failure (Hawkins and Shenoi 1993; Phillips and Shenoi 1998; Dharmawan et al. 2008; Nimje and Panigrahi 2015).

The structural reliance over such a specific and localised joint has, therefore, prompted research into the various configurations available, and the peel strength associated with these (Stickler and Ramulu 2006). This was deemed particularly relevant given the out-of-plane nature of T-joints, compared to the extensively studied in-plane composite joints (Matthews et al. 1982; Crammond et al. 2014; Xu et al. 2016). Early work provided an initial assessment of the breadth of options for T-joints (Hawkins and Shenoi 1993; Theotokoglou and Moan 1996; Phillips and Shenoi 1998; Shenoi and Dodkins 2000; Dulieu-Barton et al. 2001). Further configurations were subsequently investigated (Toftegaard and Lystrup 2005; Diler et al. 2009; Di Bella et al. 2010), ultimately leading to a smaller range of commonly employed configurations (Greene 2014) being included in structural regulations such as ISO 12215-6 (ISO 2018), namely: (a) resin fillets (also known as glueing on both sides under ISO 12215-6 (ISO 2018) terminology); (b) bonding angles (also known as tabbing

on both sides in ISO 12215-6 (ISO 2018) or overlamination); and, (c) bonding angles with fillets. These configurations are depicted in Figure 1(a–c), respectively. While resin fillets benefit from simplicity and low cost, their structural strength is known to be inferior to that of overlaminated configurations, such as bonding angles and bonding angles with fillets (Theotokoglou and Moan 1996; Dulieu-Barton et al. 2001; Di Bella et al. 2010). In recent years, an increasingly employed configuration emerged, namely, bonding ties, as shown in Figure 1(d), and now included in Lloyd's Special Service Crafts rules (Lloyd's Register 2023). However, the peel strength of T-joints employing bonding ties remains to be experimentally characterised, and any benefit over existing configurations (such as bonding angles with and without fillets) is yet to be quantified.

The applications of T-joints extend to a wide range of industrial applications, particularly aerospace (Apalak et al. 1996) where, for instance, T-joints are employed to prevent skin buckling on airplane wings (Nimje and Panigrahi 2015). Aerospace applications, however, are characterised by the use of single skin joints (Chuyang and Xiong 2012; Burns et al. 2016) and the use of fasteners (Guo and Li 2020). The use of single-skin joints and fasteners is in contrast with marine applications. As such, the scope of this paper is focused on cored bulkheads, where two core materials are investigated, namely, foam and honeycomb. The former has been the focus of all previous experimental studies, but honeycomb T-joints remain uncharacterised but for the experiments on bonded (no fillets) T-joints of Khosravani and Weinberg (2018). Further motivation for the use of cored bulkhead and plating is their greater sustainability compared to single skin laminates (Han et al. 2024).

Consequently, this paper aims to further the understanding of composite T-joints for marine applications by addressing two outstanding research questions, namely (1) the behaviour of the

CONTACT Jean-Baptiste R. G. Souppez j.souppez@aston.ac.uk Mechanical, Biomedical and Design Engineering Department, School of Engineering and Technology, College of Engineering and Physical Sciences, Aston University, Astron Street, Birmingham, B4 7ET, UK

Figure 1. Schematics of the regulatory T-joints investigated in this study, namely, (a) resin fillets, (b) bonding angles, (c) bonding angles with fillets, and (d) bonding ties. Not to scale.

emerging bonding ties configurations compared to resin fillets, bonding angles and bonding angles with fillets; and (2) compare the peel strength of foam-cored and honeycomb-cored bulkheads for the four T-joint configurations commonly employed and present in rules and regulations, as depicted in Figure 1. To answer the aforementioned research questions, destructive testing is undertaken on resin fillets, bonding angles, bonding angles with fillets and bonding ties T-joints, with both a foam and a honeycomb core, subject to a tensile load, in line with ISO 527-4 (ISO 2018).

The remainder of this paper is structured as follows. First, Section 2 details the materials employed and manufacturing of the T-joints, the experimental testing setup and protocol, and the quantification of mechanical properties and their associated uncertainty. Then, Section 3 presents the results for the four T-joint types investigated, for both foam-cored and honeycomb-cored bulkheads. Lastly, the main findings are summarised in Section 4.

2. Methodology

2.1. Materials and manufacturing

The sandwich panels were manufactured feature an inner and outer skin, each made of two $410\,\mathrm{g\,m^{-2}}$ stitched bi-axial pre-preg carbon fibre at $0°$-$90°$, encapsulated in epoxy resin, either side of a 15 mm styrene acrylonitrile (SAN) foam core (Corecell M80, density $\rho = 85\,\mathrm{kg\,m^{-3}}$) for the base plating, and a 25 mm SAN foam core (Corecell M80) or 25 mm honeycomb core (Nomex aramid, $\rho = 64\,\mathrm{kg\,m^{-3}}$) for the bulkheads. The laminate is intended to be representative of a high-performance craft, hence the use of carbon fibre pre-prep and advanced cores. The vessel size could range from the higher end of small crafts under (ISO 2019) to the lower end of large yachts under (Lloyd's Register 2023). As such, the findings are relevant to a wide range of high-performance vessels.

To ensure the manufacturing consistency of all T-joints, the panels were waterjet cut to achieve a constant 50 mm width. Additionally, the rough side of the base horizontal components, created by the peel-ply, was always oriented upwards to promote better bonding. For the vertical elements, both sides are roughened with 120-grit sandpaper and cleaned before bonding. A custom jig was employed to clamp horizontal and vertical components in place during the manufacturing process of the T-joints to guarantee their orthogonality. Three plies of $240\,\mathrm{g\,m^{-2}}$ carbon fibre tape, 50 mm wide, were employed as tabbing for bonding angles (with and without fillets) and bonding ties. These were hand laminated using epoxy resin, with a peel-ply applied to help maintain a consistent fibre weight fraction and thus not impact the properties of the laminate (Han et al. 2023). All T-joints were manufactured by the same operator and in the same laboratory conditions to ensure consistent manufacturing quality.

The tabbing followed the regulatory 50 mm + 25 mm/ply (ISO 2018; Lloyd's Register 2023), namely, 50 mm for the first ply followed by an additional 25 mm for subsequent plies, i.e. 75 mm and

100 mm for the second and third plies, respectively. These dimensions apply to both the horizontal and vertical components and both sides of the T-joint. The same layup was applied for bonding ties. Tabbing and bonding ties were hand laminated using laminating epoxy resin, with a peel-ply applied to the tabbing in order to remove any excess resin and ensure a consistent finish. For the resin fillets and bonding angles with fillets, laminating epoxy resin was thickened using 7 g of fumed silica thixotropic powder per 100 g of resin, and a 10 mm radius was employed. For all honeycomb-cored samples, thickened epoxy was also used to fill the honeycomb cells to maximise the glueing with the base plate. The details of the four configurations employed are shown in Figure 2.

2.2. Experimental setup

All experiments were conducted on an Instron 5965 fitted with a 5 kN load cell and conducted at temperatures $24.0°\mathrm{C} \leq T \leq 25.0°\mathrm{C}$ as well as relative humidities $0.37 \leq \varphi \leq 0.38$. The custom-built test rig, depicted in Figure 3, features a 340 mm distance between the inside of the clamping points, also employed by Li et al. (2006), where the horizontal plating is secured using 30 mm long clamps, accommodating the 50 mm wide T-joints. The vertical component (bulkhead) is subject to uniaxial tension applied at a displacement rate of $2\,\mathrm{mm\,min^{-1}}$, with a 1 N preload triggering acquisition at 100 Hz. These test parameters are as specified in ISO 527-4:2019 (ISO 2023), which is recommended for the tensile test of composites for marine applications (Souppez 2018b) and dictated by the ISO 12215-5, applicable to both recreational and commercial crafts (Souppez 2018a, 2019).

2.3. Mechanical properties and uncertainty quantification

From the recorded force F and displacement ΔL, the strain ϵ and the stress σ are computed as, respectively

$$\epsilon = \frac{\Delta L}{L_0}, \tag{1}$$

and

$$\sigma = \frac{F}{bl_b}, \tag{2}$$

where $L_0 = 250$ mm is the gauge length, $b = 50$ mm is the width of the samples, and l_b is the total bonding width in contact with the base plate (varying for each configuration). In this instance, the resin fillet would yield a much lower l_b than all other configurations. Consequently, the peel strength per unit of bonding length, σ_p, expressed in N mm^{-1}, is defined as

$$\sigma_p = \frac{F_{\max}}{l_b}, \tag{3}$$

where $F_{\max}$ is the maximum force prior to yield.
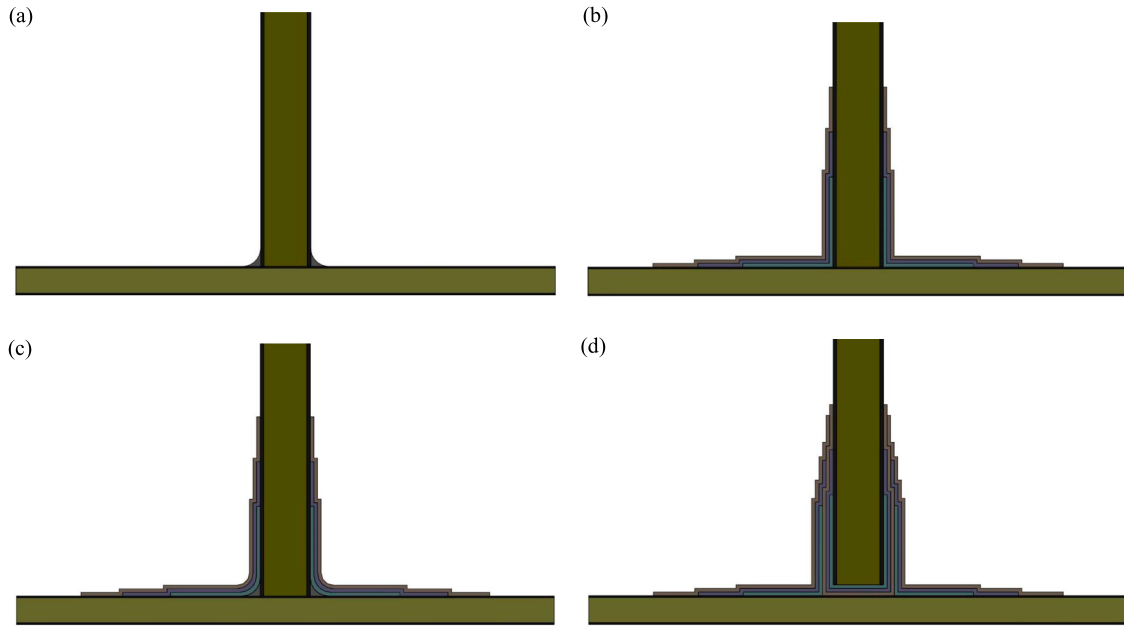
Figure 2. Details, to scale, of the T-joints materials and dimensions investigated in this study, namely, (a) resin fillets, (b) bonding angles, (c) bonding angles with fillets, and (d) bonding ties.
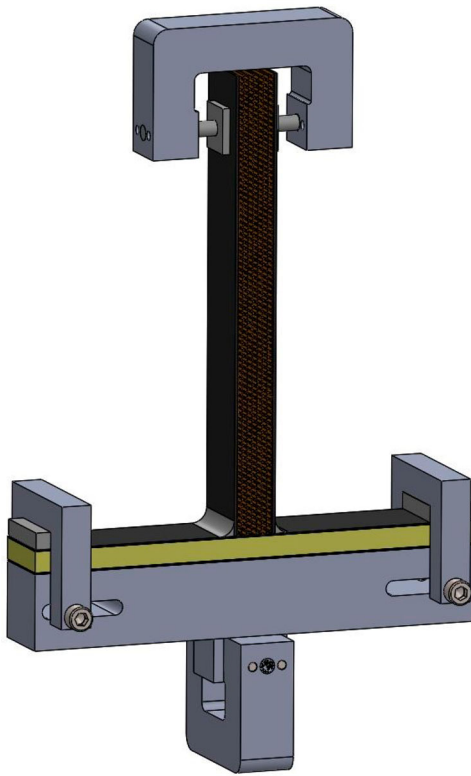
Figure 3. Schematic of the custom jig for the experimental setup for the mechanical testing of T-joints.

Table 1. Summary of the bias limits.

Quantity	Bias limit
Elongation, $B(\Delta L_0)$ [mm]	0.00005
Length, $B(L_0)$ [mm]	0.5
Force, $B(F)$ [N]	0.00005
Width, $B(b)$ [mm]	0.005
Bonding length, l_b [mm]	0.005

The uncertainty U of the results presented in Section 3 is quantified using the methodology for composite materials detailed in Souppez and Laci (2022), namely,

$$U = \sqrt{(B^2 + P^2)}, \qquad (5)$$

where B is the bias and P is the precision.

For a quantity X based on a number N of independent variables x_i with a bias limits $B(x_i)$, the bias $B(X)$ is (Moffat 1988; JCGM 2008)
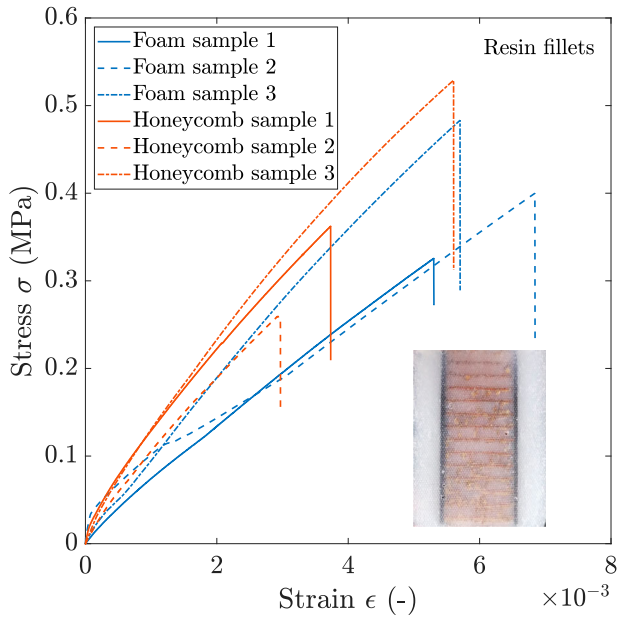
$$B(X) = \left[\sum_{i=1}^{N} \left(\frac{\partial X}{\partial x_i} B(x_i) \right)^2 \right]^{\frac{1}{2}}, \qquad (6)$$

with bias limits listed in Table 1.

Based on the standard deviation σ_{dev} at the 95% confidence level, i.e. $t_{95} = 4.303$ for the $n = 3$ repeats (also employed by Tofte-gaard and Lystrup (2005), Guo and Morishima (2011) and Guo and Li (2020) for T-joints), the precision is given as

$$P_r = \frac{t_{95}\sigma_{\text{dev}}}{\sqrt{n}}. \qquad (7)$$

The statistical significance of the results is ascertained using analysis of variance (ANOVA) and the honestly significant difference (HSD), as defined by Tukey (1991). In this work, statistical significance will be considered for $p < 0.05$ and will be used as part of the discussion in Section 3.5.

The modulus E is quantified using the linear least squares method for $0.001 \leq \epsilon \leq 0.005$ with the upper bounder of ϵ reduced by the minimum amount to achieve a coefficient of determination $R^2 \geq 0.99$ where necessary, with E computed as

$$E = \frac{\sigma}{\epsilon}. \qquad (4)$$

Figure 4. Stress–strain curves for the foam-cored ($n = 3$) and honeycomb-cored ($n = 3$) T-joints with resin fillets. Inset shows a failed (debonded) vertical component of a honeycomb T-joint.

Figure 5. Stress–strain curves for the foam-cored ($n = 3$) and honeycomb-cored ($n = 3$) T-joints with bonding angles. Inset shows typical failure behaviour.

3. Results

3.1. Resin fillets

The stress–strain curves for the 10 mm resin fillets configuration are presented in Figure 4. All failures are abrupt and characterised by a sharp debonding of the adhesive and radii from the base for all test samples (see inset in Figure 4). Qualitatively, honeycomb-cored samples display a steeper slope (i.e. E), albeit with a lower yield strain than foam-cored samples. Notably, the results are characterised by high variations, which would incur higher factors of safety for design purposes and is reflected in the uncertainty of the results.

Indeed, while average values for the yield strength ($\sigma_y = 0.402$ MPa ± 0.161 MPa for foam compared to that of honeycomb $\sigma_y = 0.383$ MPa ± 0.276 MPa) and peel strength ($\sigma_p = 17.37$ N mm^{-1} ± 3.63 N mm^{-1} for foam compared to $\sigma_p = 18.26$ N mm^{-1} ± 13.08 N mm^{-1} for honeycomb) are comparable, the uncertainty is significant for resin fillets. Differences are noticed both for the modulus, with $E = 88.76$ MPa ± 5.38 MPa for honeycomb compared to a lesser $E = 60.26$ MPa ± 17.37 MPa for foam, and the yield strain, where a higher value of $\epsilon_y = 0.0059 \pm 0.0017$ is exhibited by foam compared to honeycomb where $\epsilon_y = 0.0041 \pm 0.0027$. The latter is hypothesised as the higher likelihood of a weaker bond for the honeycomb (despite the thickened epoxy applied to fill the honeycomb cells). Indeed, all honeycomb sample failures occurred along the glue line, with no honeycomb left glued to the base plate. This is in contrast with foam samples, where foam remained glued to the base plate after failure.

Despite their ease of manufacture, resin fillets are omitted in favour of configurations with tabbing, such as bonding angles (see Section 3.2), bonding angles with fillets (see Section 3.3), and bonding ties (see Section 3.4).

3.2. Bonding angles

Standard tabbing, as defined in both ISO (2018) and Lloyd's Register (2023) is employed, namely, 50 mm + 25 mm/ply, for the bonding angles configuration, for which the stress–strain curves are depicted
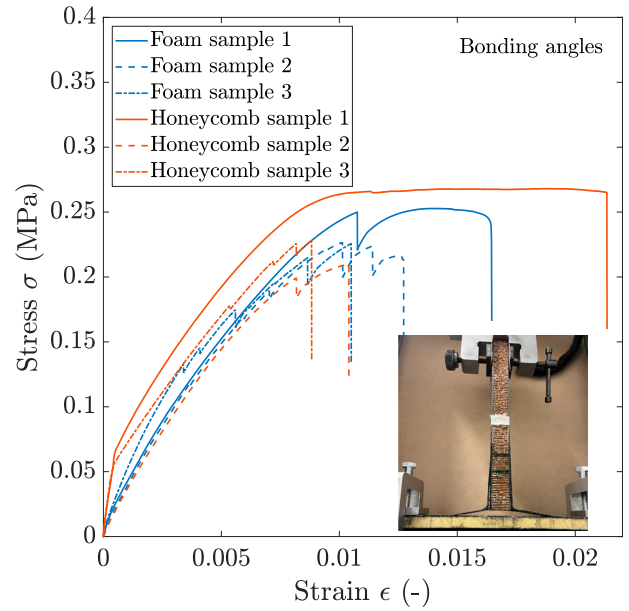
in Figure 5. A notable change in behaviour compared to resin fillets is noticed: the abrupt failure of resin fillets is now replaced with a progressive failure. Following the elastic deformation region, debonding of the tabbing occurs, with failure strain far exceeding yield strain (see inset in Figure 5).

Any differences in mechanical properties between the two cores remain within the bounds of the uncertainty quantified, with comparable yield strength ($\sigma_y = 0.193$ MPa ± 0.086 MPa for foam and $\sigma_y = 0.209$ MPa ± 0.044 MPa for honeycomb), yield strain ($\epsilon_y = 0.0072 \pm 0.0050$ for foam and $\epsilon_y = 0.0094 \pm 0.0039$ for honeycomb), modulus ($E = 29.30$ MPa ± 4.40 MPa for foam and $E = 26.54$ MPa ± 1.39 MPa for honeycomb), and, importantly, peel strength ($\sigma_p = 24.63$ N mm^{-1} ± 10.98 N mm^{-1} for foam compared to $\sigma_p = 26.70$ N mm^{-1} ± 5.61 N mm^{-1} for honeycomb). The latter represents a 41.73% and a 46.24% increase compared to the fillet radius for foam and honeycomb, respectively.

Bonding angles are, therefore, a marked improvement compared to resin fillets to increase the peel strength. However, this configuration evidenced an onset of delamination in the sharp corners between the horizontal and vertical panels. Consequently, the introduction of a fillet in that critical location should enhance the overall peel strength of the T-joints. This hypothesis is verified in the following Section.

3.3. Bonding angles with fillets

The bonding angles with fillets configuration are identical to the bonding angles in terms of its tabbing arrangement, but features the addition of 10 mm radii, thereby enabling to study the effect of such a small change. The stress–strain curves are shown in Figure 6.

The addition of the fillets results in a notable increase in yield strength, namely, $\sigma_y = 0.231$ MPa ± 0.036 MPa for foam and $\sigma_y = 0.228$ MPa ± 0.061 MPa for honeycomb. Moreover, the peel strength increases by 38.46% for foam to $\sigma_p = 34.10$ N mm^{-1} ± 5.38 N mm^{-1} and by 26.00% for honeycomb to $\sigma_p = 33.64$ N mm^{-1} ± 9.08 N mm^{-1} compared to bonding angles alone. On the other hand, both yield strain ($\epsilon_y = 0.0098 \pm 0.0021$ for foam and $\epsilon_y = 0.0086 \pm 0.0013$ for honeycomb) and modulus ($E =$
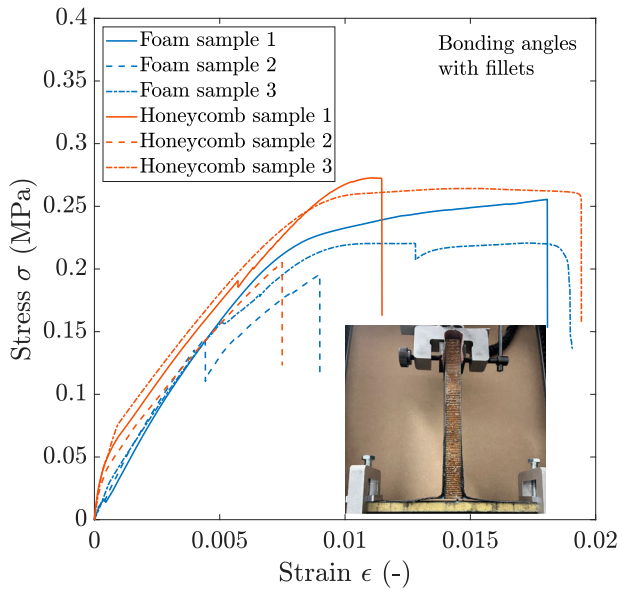
Figure 6. Stress–strain curves for the foam-cored ($n = 3$) and honeycomb-cored ($n = 3$) T-joints with bonding angles with fillets. Inset shows typical failure behaviour.

Figure 7. Stress–strain curves for the foam-cored ($n = 3$) and honeycomb-cored ($n = 3$) T-joints with bonding ties. Inset shows typical failure behaviour.

32.26 MPa $\pm$ 1.35 MPa for foam and $E = 25.54$ MPa $\pm$ 0.70 MPa for honeycomb) remain comparable to bonding angles.

As such, the peel strength can be greatly improved with the addition of a fillet radius to bonding angles, alleviating the drawback of a sharp right angle joint. Whether the emerging bonding ties configuration, as now featured by Lloyd's Register (2023), is advantageous compared to bonding angles with fillets is ascertained next.
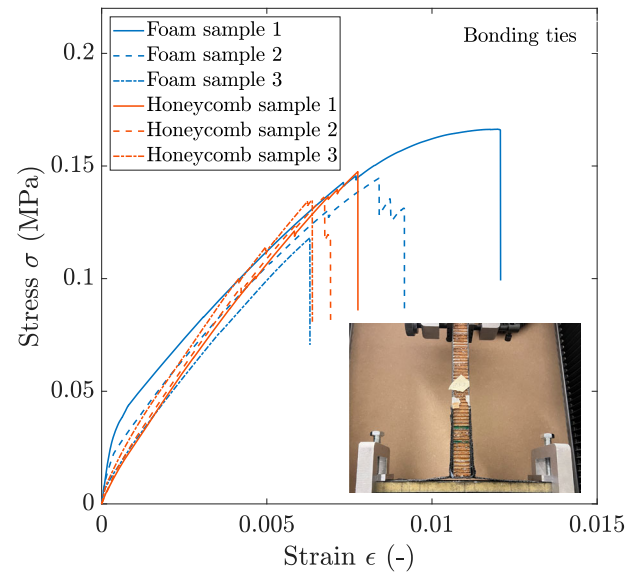
3.4. Bonding ties

In this section, the first experimental results for T-joints employing the bonding ties configuration are presented, with Figure 7 presenting the stress–strain curves for the tested samples. Despite the presence of the same tabbing as for bonding angles (Section 3.2) and bonding angles with fillets (Section 3.3), the failure behaviour is much closer to that on resin fillets (Section 3.1) with an abrupt failure (see inset in Figure 7). The failure consistently took place at the base on the bonding ties (i.e. under the vertical element) and led to central debonding of the tabbing, which, however, remained bonded to the horizontal plates at the far ends. As such, it is the adhesion between the bonding ties and plating that causes the early and abrupt failure.

Remarkably, the peel strength of bonding ties is almost identical to that of resin fillets (Section 3.3), with values of $\sigma_p = 18.05$ N mm^{-1} $\pm$ 5.53 N mm^{-1} for foam and $\sigma_p = 17.73$ N mm^{-1} $\pm$ 1.82 N mm^{-1} for honeycomb. As such, implementation of this configuration would not be recommended, owing to the additional cost of material and labour, as well as its increased complexity compared to resin fillets for no superior peel strength.

The remainder of the mechanical properties are as follows. The yield strength is $\sigma_y = 0.141$ MPa $\pm$ 0.043 MPa for foam and $\sigma_y = 0.139$ MPa $\pm$ 0.014 MPa for honeycomb, the yield strain is $\epsilon_y = 0.0081 \pm 0.0035$ for foam and $\epsilon_y = 0.0070 \pm 0.0015$ for honeycomb, and the modulus is $E = 17.29$ MPa $\pm$ 0.73 MPa for foam and $E = 21.22$ MPa $\pm$ 0.31 MPa for honeycomb.

Ultimately, the following ranking can be established to maximise the peel strength of composite T-joints: first, bonding angles with fillets, then bonding angles, and last, both resin fillets and bonding ties.

3.5. Discussion

Sections 3.1–3.4 quantified the mechanical properties of foam and honeycomb T-joints for four configurations. A summary of the mechanical properties ascertained is provided in Table 2, which enables to answer the two main research questions tackled in this work, namely, investigating the bonding ties configuration and whether foam or honeycomb core affect the peel strength. Statistical analysis of the results based on ANOVA and HSD is employed to distinguish results that are statistically significant from those that are not in Table 2.

Firstly, the peel strength of composite T-joint configurations yields very clear results, particularly with respect to bonding ties which is shown not to provide any benefits compared to resin fillets, both characterised by an abrupt debonding failure. Bonding angles represent a marked improvement, with further opportunities to improve the peel strength with the addition of fillets to the bonding angles.

Secondly, within the uncertainty of the present experiments and based on the statistical analysis undertaken, the peel strength is shown to be independent of the core employed. In fact, only the modulus presents a statistically relevant dependency on the core employed. However, given peel strength is the main design requirement for such joints, the nature of the core does not appear to affect the results. It is noted that, while this work reports the average values an in-depth quantification of the uncertainty (see Section 2.3), for design purposes, it is established practice under ISO standards (ISO 2023) to retain the lesser of 90% of the mean or the mean minus two standard deviations for any given properties.

4. Conclusions

Experimental testing of composite T-joints has been undertaken, owing to their crucial role in composite structures. Two core materials were investigated, namely, foam and honeycomb, the latter having received comparatively far less attention. Furthermore, four distinct configurations were investigated, namely, resin fillets, bonding angles, bonding angles with fillets and bonding ties. The latter is a recent and emerging configuration, recently recognised by class rules, but previously never investigated experimentally.

Table 2. Summary of the mechanical properties for the T-joint configurations investigated.

Configuration		Resin fillets	Bonding angles	Bonding angles with fillets	Bonding ties
Peel strength, σ_p [N mm^{-1}]	Foam	17.37 ± 3.63[c]	24.63 ± 10.98[b]	34.10 ± 5.38[a]	18.05 ± 5.53[c]
	Honeycomb	18.26 ± 13.08[c]	26.70 ± 5.61[b]	33.64 ± 9.08[a]	17.73 ± 1.82[c]
Yield stress, σ_y [MPa]	Foam	0.402 ± 0.161[a]	0.193 ± 0.086[bc]	0.231 ± 0.036[b]	0.141 ± 0.043[c]
	Honeycomb	0.383 ± 0.276[a]	0.209 ± 0.044[b]	0.228 ± 0.061[b]	0.139 ± 0.014[c]
Yield strain, ϵ_y [-]	Foam	0.0059 ± 0.0017[b]	0.0072 ± 0.0050[ab]	0.0098 ± 0.0021[a]	0.0081 ± 0.0035[a]
	Honeycomb	0.0041 ± 0.0027[b]	0.0094 ± 0.0039[a]	0.0086 ± 0.0013[a]	0.0070 ± 0.0015[a]
Modulus, E [MPa]	Foam	60.26 ± 17.37[a]	29.30 ± 4.40[b]	32.26 ± 1.35[b]	17.29 ± 0.73[c]
	Honeycomb	88.76 ± 5.38[a]	26.54 ± 1.39[b]	25.54 ± 0.70[b]	21.22 ± 0.31[c]

Note: On any given row, common letters indicate values that are not significantly different based on HSD at the 5% level of significance ($p < 0.05$).

The bonding ties configuration did not yield and structural benefit compared to resin fillets, achieving an identical peel strength, within the uncertainty of the present results, for both cores. In comparison to a foam-cored bonding ties configuration, bonding angles result in a 36.46% increase in peel strength, while bonding angles with fillets yielded an 88.94% increase in peel strength. For a honeycomb-cored T-joint, these figures rise to 50.56% for bonding angles and 89.70% for bonding angles with fillets compared to bonding ties, respectively. As such, bonding angles with fillets appear as the optimum configuration, and bonding ties are discouraged owing to their inferior peel strength despite a greater complexity, labour cost and material cost, the latter leading to a heavier mass.

While limited work has been conducted on honeycomb-cored T-joints, the present work provides the first experimental data for such material, thereby paving the way for future numerical validation. Interestingly, with thickened epoxy filling the honeycomb cells in contact with the base plate, identical results between foam and honeycomb core are achieved for the peel strength for the test configurations, within the experimental uncertainty of this work.

These results provide novel insights into the strength and failure behaviour of T-joints for high-performance, cored panels in marine applications. It is anticipated these findings may inform the development of future structural designs and associated rules and regulations (e.g. ISO 12215-5), while also providing a relevant experimental benchmark for future numerical analyses, which may, for instance, provide a parametric characterisation of the design parameters associated with T-joints. These may include the effect of the bonding radius, tabbing and materials.

Acknowledgments

Disclosure statement

No potential conflict of interest was reported by the author(s).

Data availability statement

Data can be made available upon reasonable request.

ORCID

Jean-Baptiste R. G. Souppez http://orcid.org/0000-0003-0217-5819

References

Apalak ZG, Apalak MK, Davies R. 1996. Analysis and design of tee joints with double support. Int J Adhes Adhes. 16(3):187–214. doi: 10.1016/0143-7496(96)87013-8

Bai JB, Dong CH, Xiong JJ, Luo CY, Chen D. 2019. Progressive damage behaviour of RTM-made composite T-joint under tensile loading. Compos B Eng. 160:488–497. doi: 10.1016/j.compositesb.2018.12.069

Burns L, Mouritz A, Pook D, Feih S. 2016. Strengthening of composite T-joints using novel ply design approaches. Compos B Eng. 88:73–84. doi: 10.1016/j.compositesb.2015.10.032

Chuyang L, Xiong J. 2012. Static pull and push bending properties of RTM-made TWF composite tee-joints. Chin J Aeronaut. 25(2):198–207. doi: 10.1016/S1000-9361(11)60379-8

Crammond G, Boyd S, Dulieu-Barton J. 2014. Dynamic analysis of composite marine structures using full-field measurement techniques. J Mar Eng Technol. 13:23–35. doi: 10.1080/20464177.2014.11020290

Delzendehrooy F, Akhavan-Safar A, Barbosa A, Beygi R, Cardoso D, Carbas R, Marques E, Da Silva L. 2022. A comprehensive review on structural joining techniques in the marine industry. Compos Struct. 289:115490. doi: 10.1016/j.compstruct.2022.115490

Dharmawan F, Li H, Herszberg I, John S. 2008. Applicability of the crack tip element analysis for damage prediction of composite T-joints. Compos Struct. 86(1-3):61–68. doi: 10.1016/j.compstruct.2008.03.030

Dharmawan F, Thomson RS, Li H, Herszberg I, Gellert E. 2004. Geometry and damage effects in a composite marine T-joint. Compos Struct. 66(1-4):181–187. doi: 10.1016/j.compstruct.2004.04.036

Di Bella G, Borsellino C, Pollicino E, Ruisi VF. 2010. Experimental and numerical study of composite T-joints for marine application. Int J Adhes Adhes. 30(5):347–358. doi: 10.1016/j.ijadhadh.2010.03.002

Diler EA, Özes Ç, Neşer G. 2009. Effect of T-joint geometry on the performance of a GRP/PVC sandwich system subjected to tension. J Reinf Plast Compos. 28(1):49–58. doi: 10.1177/0731684407081378

Dulieu-Barton J, Earl J, Shenoi R. 2001. Determination of the stress distribution in foam-cored sandwich construction composite tee joints. J Strain Anal Eng Des. 36(6):545–560. doi: 10.1243/0309324011514700

Greene E. 2014. Marine composites non-destructive evaluation. Ship Struct. 1:416–427.

Guo S, Li W. 2020. Numerical analysis and experiment of sandwich T-joint structure reinforced by composite fasteners. Compos B Eng. 199:108288. doi: 10.1016/j.compositesb.2020.108288

Guo S, Morishima R. 2011. Numerical analysis and experiment of composite sandwich T-joints subjected to pulling load. Compos Struct. 94(1):229–238. doi: 10.1016/j.compstruct.2011.06.022

Han Z, Jang J, Souppez JBRG, Lim M, Oh D. 2024. Environmental implications of a sandwich structure of a glass fiber-reinforced polymer ship. Ocean Eng. 298:117122. doi: 10.1016/j.oceaneng.2024.117122

Han Z, Jang J, Souppez JBRG, Seo HS, Oh D. 2023. Comparison of structural design and future trends in composite hulls: a regulatory review. Int J Nav Archit Ocean Eng. 15:100558. doi: 10.1016/j.ijnaoe.2023.100558

Hawkins G, Shenoi R. 1993. A parametric study to determine the influence of geometric variations on the performance of a bulkhead to shell plating joint. ICCM/9. Compos Des. 4:97–104.

ISO. 2018. ISO 12215-6:2018 – Small craft – Hull construction and scantlings – Part 6: Structural arrangements and details. Technical Report. International Organization for Standardization. Geneva, Switzerland.

ISO. 2019. SO 12215-5:2019 – Small craft–Hull construction and scantlings – Part 5: Design pressures for monohulls, design stresses, scantlings determination. Technical Report. International Organization for Standardization. Geneva, Switzerland.

ISO. 2023. ISO 527-4:2023 – Plastics–Determination of tensile properties – Part 4: Test conditions for isotropic and orthotropic fibre-reinforced plastic composites. Technical Report. International Organization for Standardization. Geneva, Switzerland.

JCGM (2008). JCGM 100:2008, Evaluation of measurement data–Guide to the expression of uncertainty in measurement. Technical Report. Joint Committee for Guides in Metrology. Pavillon de Breteui, France.

Khosravani MR, Weinberg K. 2018. Characterization of sandwich composite T-joints under different ageing conditions. Compos Struct. 197:80–88. doi: 10.1016/j.compstruct.2018.05.043

Li H, Dharmawan F, Herszberg I, John S. 2006. Fracture behaviour of composite maritime T-joints. Compos Struct. 75(1-4):339–350. doi: 10.1016/j.compstruct.2006.04.052

Lloyd's Register (2023). Rules and Regulations for the Classification of Special Service Craft. Technical Report. Lloyd's Register. London, UK.

Matthews F, Kilty P, Godwin E. 1982. A review of the strength of joints in fibre-reinforced plastics. Part 2. Adhesively bonded joints. Composites. 13(1):29–37. doi: 10.1016/0010-4361(82)90168-9

Moffat RJ. 1988. Describing the uncertainties in experimental results. Exp Therm Fluid Sci. 1(1):3–17. doi: 10.1016/0894-1777(88)90043-X

Nimje S, Panigrahi S. 2015. Interfacial failure analysis of functionally graded adhesively bonded double supported tee joint of laminated FRP composite plates. Int J Adhes Adhes. 58:70–79. doi: 10.1016/j.ijadhadh.2015.01.002

Phillips H, Shenoi R. 1998. Damage tolerance of laminated tee joints in FRP structures. Compos A Appl Sci Manuf. 29(4):465–478. doi: 10.1016/S1359-835X(97)00081-X

Shenoi R, Dodkins A. 2000. Design of ships and marine structures made from FRP composite materials. In: Kelly A, Zweben C editors. Comprehensive composite materials. Pergamon: Oxford; p. 429–449.

Souppez JBRG. 2018a. Structural analysis of composite search and rescue vessels under the new BS EN ISO 12215-5. In: SURV9–Surveillance, Search and Rescue Craft. London: Royal Institution of Naval Architects.

Souppez JBRG. 2018b. Structural design of high performance composite sailing yachts under the new BS EN ISO 12215-5. J Sail Technol. 3(1):1–18. doi: 10.5957/jst.2018.02

Souppez JBRG. 2019. Designing the next generation of small pleasure and commercial powerboats with the latest ISO 12215-5 for hull construction and scantlings. In: 1st SNAME/IBEX Symposium, Society of Naval Architects and Marine Engineers; Tampa, FL.

Souppez JBRG, Laci J. 2022. Ultimate strength of quasi-isotropic composites: ISO 12215-5: 2019 validation. Int J Mar Eng. 164:237–246. doi: 10.5750/ijme.v164iA2.1178

Stickler P, Ramulu M. 2006. Experimental study of composite T-joints under tensile and shear loading. Adv Compos Mater. 15(2):193–210. doi: 10.1163/156855106777873914

Theotokoglou EE, Moan T. 1996. Experimental and numerical study of composite T-joints. J Compos Mater. 30(2):190–209. doi: 10.1177/002199839603000 2

Toftegaard H, Lystrup A. 2005. Design and test of lightweight sandwich T-joint for naval ships. Compos A Appl Sci Manuf. 36(8):1055–1065. doi: 10.1016/j.compositesa.2004.10.031

Truelock D, Lavroff J, Pearson D, Czaban Z, Luo H, Wang F, Catipovic I, Begovic E, Takaoka Y, Loureiro C, et al. 2022. Committee v. 5: Special vessels. In: International Ship and Offshore Structures Congress; Vancouver, Canada. SNAME; p. D011S001R006.

Tukey JW. 1991. The philosophy of multiple comparisons. Stat Sci. 6(1):100–116. doi: 10.1214/ss/1177011945

Xu S, Zhang Y, Duan M, Dai B. 2016. Research on the shear stress of single-lap joints using a variational method. J Mar Eng Technol. 15(1):9–18. doi: 10.1080/20464177.2016.1139652